



Design of a Reconfigurable Parallel Continuum Robot With Tendon-Actuated Kinematic Chains

Georg Böttcher, Sven Lilge , *Student Member, IEEE*, and Jessica Burgner-Kahrs , *Senior Member, IEEE*

Abstract—In this letter, a novel spatial parallel continuum robot is proposed. It is composed of three tendon-actuated continuum robots as kinematic chains that are coupled at a common end-effector platform by spherical joints. A modular design approach is used, allowing the reconfiguration of each continuum robot's base position and orientation to adapt the overall structure to application specific constraints and environments. The parallel continuum robot is evaluated in terms of its position and orientation repeatability. Furthermore, comparisons are made to the performance of the single continuum kinematic chains. Overall, average position and orientation repeatabilities of 3.3 mm and 1.2° can be achieved for the parallel continuum robot, with a single individual continuum segment showing repeatabilities of 5.5 mm and 3.2°. The proposed parallel continuum robot exhibits improved repeatabilities than each of the employed individual continuum segments, improving the average repeatability by 67% for position and 167% for orientation, respectively.

Index Terms—Continuum robots, mechanical design, parallel robots.

I. INTRODUCTION

CONTINUUM robots represent a growing field in robotics research. These robots are characterized by their high flexibility, inherent compliance and jointless structure. Those properties are often stated as the main advantages in comparison to conventional serial robots, as they enable continuum robots to follow non-linear trajectories and allow safe contact interaction with sensitive environments. Due to their miniaturizability, possible application areas are mainly motivated in the field of minimal invasive surgery [1].

However, the stated inherent characteristics of continuum robots also lead to some limitations and drawbacks. The relatively low stiffness of the robots makes it challenging to apply forces to manipulate and interact with the environment. Furthermore, the rather complex actuation principles used in continuum robots lead to lower accuracies and slower dynamic behaviors in comparison to conventional serial robots, especially when considering long continuum robots that offer several degrees of freedom.

Manuscript received October 14, 2020; accepted January 25, 2021. Date of publication February 5, 2021; date of current version February 19, 2021. This letter was recommended for publication by Associate Editor U.-X. Tan and Editor L. Pallottino upon evaluation of the reviewers' comments. (*Corresponding author: Sven Lilge.*)

The authors are with the Continuum Robotics Laboratory, Department of Mathematical and Computational Sciences, University of Toronto Mississauga, Mississauga L5L 1C6, Canada (e-mail: georg.a.boettcher@gmail.com; slilge@cs.toronto.edu; jbk@cs.toronto.edu).

Digital Object Identifier 10.1109/LRA.2021.3057557

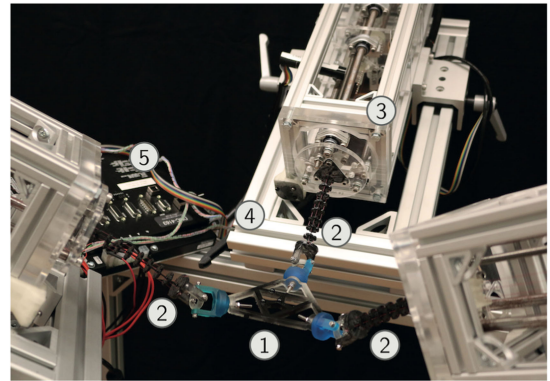


Fig. 1. Reconfigurable parallel continuum robot prototype composed of an end-effector ① connected to three continuum robots ②, each with an actuation unit ③, a spatial adjustment mechanism ④ and a motor controller ⑤.

To overcome some of these limitations, recent research advances have focused on parallel continuum robots (PCR). In such cases, multiple continuous structures are physically coupled to a common end-effector platform to increase the overall system stiffness. In comparison to regular continuum robots, each kinematic chain of the resulting parallel structure can be relatively simple and short, which can increase kinematic performances in terms of accuracy and dynamics. While each individual kinematic chain might only offer a limited number of degrees of freedom, the coupling forces between the employed continuum robots combined with the inherent passive bending degrees of freedom lead to more advanced motion capabilities for the overall structure. In this work, a novel spatial PCR is proposed. It consists of three individual continuum robots that are actuated using tendons and coupled at a common end-effector platform through spherical joints (see Fig. 1).

Generally, PCR can be treated as a special type of parallel robot, which is an exhaustive research area covering a variety of different topics such as manipulator design [2], kinematic analysis [3] and stiffness optimization [4]. In the following, we are focusing on the review of the most commonly proposed parallel robot designs that are utilizing continuously bending chains. Most current PCR designs proposed in the state-of-the-art make use of continuum links or joints that passively bend due to coupling forces present in the parallel structure. For example, in [5] a continuous Gough-Stewart platform consisting of six elastic rods that are connected to a common end-effector platform is proposed. The structure is actuated by varying the

length of each rod, while they passively deform due to coupling forces in the parallel structure. This specific PCR structure is studied in the context of endoscopic applications in [6] as well as a fingertip haptic display in [7] and [8]. A passively bending planar PCR consisting of two flexible links is proposed in [9]. The links are coupled using a passive revolute joint. The robot is actuated by two revolute joints located at the proximal ends of each link, while the links deform passively, resulting in a two degrees-of-freedom (DoF) structure. A similar planar PCR is introduced in [10], consisting of three flexible links that are actuated using linear stages, again relying on passive deformation due to coupling forces. Instead of utilizing continuum links, a continuous Delta parallel robot consisting of continuum joints is presented in [11]. These joints are attached to three rigid links, connecting them to translational actuators and a common end-effector platform. The continuum joints consist of multiple flexible backbone, allowing them to bend passively. The actuation of the robot results in the translation of each serial chain's base.

In contrast to the previously discussed designs, consisting of continuum links or joints that passively deform due to coupling forces, only a few PCR designs utilize actuation principles that actively bend the employed continuum segments. One example are the soft parallel robots introduced in [12]. They are composed of multiple coupled pneumatic actuators, allowing for bending and elongation of each individual soft segment. The resulting structures exhibit higher stiffness and extended motion capabilities than a single segment soft robot. Another actively bending PCR is introduced in [13]. Multiple pneumatic actuated soft continuum robots are coupled to a common end-effector platform using spherical joints.

To summarize the state of the art in PCR, the majority of proposed designs utilize passively bending continuum links or joints. Rather than investigating them as actuated structures themselves, often conventional discrete joints, such as revolute or linear actuators, are used to actuate the parallel structures. Therefore, the full potential of continuum robots and their different possible actuation principles have not been fully utilized yet.

Tendon actuation would allow to actively bend the individual continuum segments, such that each individual kinematic chain of the resulting parallel structure can be treated as a fully functioning continuum robot itself. In addition, tendon actuation may be easier to implement and control than pneumatic actuation, which is often used in the context of actively bending PCR designs.

In this letter, we propose a spatial tendon-actuated PCR, extending our previous work on planar PCR structures [14]. Our novel PCR is composed of three tendon-actuated continuum robots and possesses nine degrees of freedom in joint space. As every continuum robot can bend in two directions and be translated using a prismatic joint at its base, the resulting PCR is a redundant system. In addition, we make use of a modular design that enables reconfiguration of each continuum robot's base position and orientation. This allows adaption of the robotic system to different application environments and constraints. In

a first set of experiments, we investigate the robotic prototype in terms of position and orientation repeatability.

II. KINEMATIC STRUCTURE

The kinematic structure of the proposed PCR is based on common tendon-actuated continuum robots (TACR) composed of a single bending segment. We consider that these TACR can bend in two directions independently using tendons routed straight along the backbone. To obtain a system with the required degrees of freedom to fully control the pose of the end-effector we couple three individual such TACRs together, resulting in six degrees of freedom. We choose a triangle as a common end-effector platform and spherical joints to couple each TACR to the platform.

We note, that the workspace of the now resulting parallel structure is mainly limited by the length and base pose of each employed continuum robot as it roughly depends on the intersection of the workspaces of each individual kinematic chain. A straightforward way to overcome this limitation is to increase the workspace of each continuum robot used. For instance, the length of a TACR could be increased in addition to concatenating multiple bending segments. Another way to increase a TACR's workspace is by introducing extensible segments [15]. However, these methods result in a more complex actuation system, that is harder to control and might introduce lower accuracies. For instance, the expected model prediction error increases along the continuum robot's length [16]. As an effective alternative, we introduce a prismatic joint to each continuum robot's base to enable translation along its central axis. Therefore, the added mechanisms remain relatively simple, which might add less inaccuracies in the overall design as discrete joints tend to be more accurate than actuated continuous structures.

While this increases the workspace of the parallel system, the introduction of three additional degrees of freedom in actuation also contributes to redundancy, as the system now possesses nine instead of just six degrees of freedom. This redundancy can be useful in applications of the manipulator, as it can possibly be exploited to fulfill secondary tasks in addition to controlling the end-effector pose. Such secondary tasks may include the avoidance of parallel singularities [17], [3] or increasing particular kinematic properties of the system such as stiffness or dexterity [18]. The resulting kinematic structure is depicted in Fig. 2.

The resulting PCR consists of three kinematic chains, each with a prismatic joint, a continuous segment that can actively bend with two degrees of freedom and a spherical joint to couple it to the end-effector platform (see Fig. 2). To describe the resulting manipulator we adapt the common notation for parallel manipulators [19]. To represent the continuous segment within the kinematic chains, we choose the letter 'F' (flexible). Since we consider actuation in bending with two degrees of freedom we add an underlined letter 'u' in brackets. We choose that letter as the universal bending in two directions offers similar degrees of freedom as a conventional universal joint, that is commonly denoted by the letter 'U'. In total, the resulting parallel structure can be denoted by 3-PFuS.

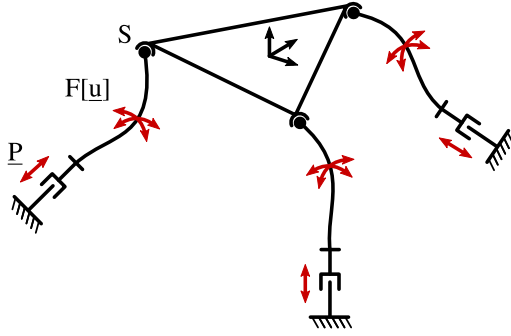


Fig. 2. Kinematic structure of the proposed 3- $\underline{P}F[u]S$ parallel continuum robot.

We note, that when investigating the mobility of the resulting system using the commonly used Grübler's formula [20], the mechanism might seem overconstrained and unable to move due to the lack of sufficient passive degrees of freedom. However, the inherent compliance of the employed continuum robots has to be taken into account, which in theory offers an infinite number of passive degrees of freedom to compensate for motions of any individual kinematic chain within the parallel structure.

III. ROBOT DESIGN

In designing a spatial tendon-actuated PCR, we set the following requirements:

- *Realize 3- $\underline{P}F[u]S$ kinematic structure* with compact actuation units per kinematic chain
- *Reconfigurability* in terms of adjustable relative base pose for each kinematic chain. This will enable future structural synthesis and kinematic analysis research on spatial tendon-actuated PCR without the necessity to build new robot prototypes.
- *Maximize workspace where possible*, as parallel robots already show limited workspaces such that each restraint reduces the workspace even further.
- *Pretensioning tendons* Tendon pretension is an important factor in TACR [21]. Low pretension can cause slack in the tendons that results in inaccuracies of the robot. High pretension can lead to buckling of the backbone which causes unpredictable behaviour of the robot's tip.

As the PCR is not subject to any target application requirement, the dimensions are a variable in the design. To explain and illustrate our proposed design, we describe the main functional units in terms of design choices in the following.

A. Tendon Actuation

In theory, three tendons are sufficient to implement bending of a TACR in two directions, each attached to a separate motor. Alternatively, four tendons connected into two independent tendon pairs, that are operated antagonistically can be used. As each tendon pair can be actuated using one motor, the total number of motors to bend the TACR in two independent directions can be reduced from three to two. This enables reduction of the robot's actuation unit size. Moreover, this allows for a more

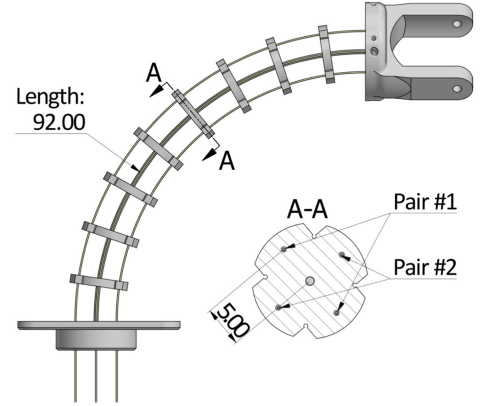


Fig. 3. Tendon-actuated continuum robot segment with cross-section of a disk depicting antagonistic tendon pairs. Major dimensions denoted in mm.

straightforward robot control. While three motors controlling two DoF always require coordination between the motors due to interdependencies in the tendon lengths, antagonistic actuation directly links a specific bending DoF to one tendon pair.

The continuum robot itself (see Fig. 3) is chosen to consist of 8 spacer disks connected to a flexible *Nitinol* backbone with a length of 92 mm. The disks have a radius of 7 mm. The tendons in a tendon pair are located on opposite sides of the backbone and both tendon pairs are rotated by 90° with respect to each other. The tendons are situated 5 mm from the backbone and are composed of 0.13 mm spectra fiber.

The two tendons in an antagonistic pair are tied to a ball chain that connects them. A custom gear (3D printed, Form 2 using Clear resin, *Formlabs, Inc., Somerville, MA, USA*) which sits on the motor shaft holds the ball chain and actuates it through the positive locking connection between the balls and depressions in its surface. This allows relatively easy assembly and disassembly of the tendon routing. There is a pitch radius of 7.5 mm between the gear's center and the ball chain's position.

The motor-gearbox-combination used (Part no. 595955, *Maxon Motor AG, Sachseln, CH*) allows for a maximum force application of 40N per tendon in connection with the gear's radius of 7.5 mm. To allow a large variety of poses, the largest expected bending angle of the continuous segment's tip was set to be 180° . During preliminary experiments, a force of 25N was determined to achieve this bending, proving the motors to be sufficient. When considering the motor's resolution in combination with the gearbox transmission and the gear's radius, the smallest actuatable length difference for each tendon pair results in $4.79 \mu\text{m}$. For motor control, *Galil DMC-4163* motion controllers (*Galil Motion Control, Rocklin, CA, USA*) are used. Target configurations are specified in joint configurations that are translated to motor ticks on which the motor encoders provide feedback to the controllers to enable precise control.

B. Pretension Mechanism

A tendon pretensioning mechanism is implemented by making the distance between the motors and the continuous segment's base adjustable. For this, the motors are mounted on

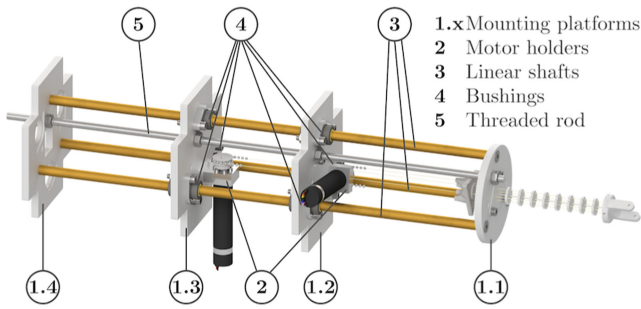


Fig. 4. Mechanism to set the pretension in the tendons by adjusting the relative motor positions through sliding mounting platforms.

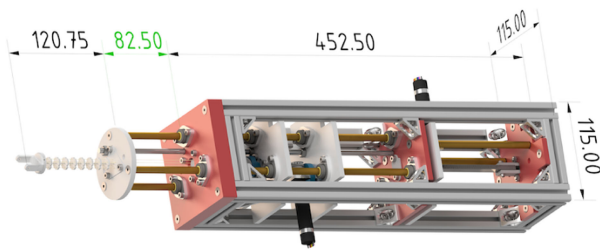


Fig. 5. Single continuum robot including linear actuation with moving platforms (white) being translated with respect to fixed platforms (red). Major dimensions denoted in mm.

PMMA platforms that can slide along linear shafts with the help of bushings. The platforms are fixed in their linear position with nuts on a threaded rod which runs through the platforms. By adjusting the position of a platform, the relative distance between the motor on the platform and the tip platform changes, leading to an adjustment of the tendon pretension. To ensure constant tendon length when the relative distance between the platforms is adjusted, 3D printed tendon re-routing parts ensure straight tendon routing between the respective platforms. The mechanism is shown in Fig. 4.

C. Linear Actuation

The additional linear DoF introduced in the robot's kinematic design has the purpose to linearly displace the continuous segment's base. In order to achieve this, the whole mechanism depicted in Fig. 4 is displaced as a rigid body. This guarantees that the adjusted pretension is independent from the linear displacement. To allow for a linear displacement of the mechanism, additional platforms and linear shafts are introduced. A gear rack and pinion (pitch radius: 5 mm) actuate the linear DoF. The gear rack is connected to the additional platforms that are held together with aluminum frames. The motor holding the pinion is held by the pretensioning mechanism's base platform. The mechanism is shown in Fig. 5. It is depicted in its maximally extended state with a maximum displacement of the continuous segment of 82.5 mm. The mechanism shown constitutes a single kinematic chain of the parallel robot.

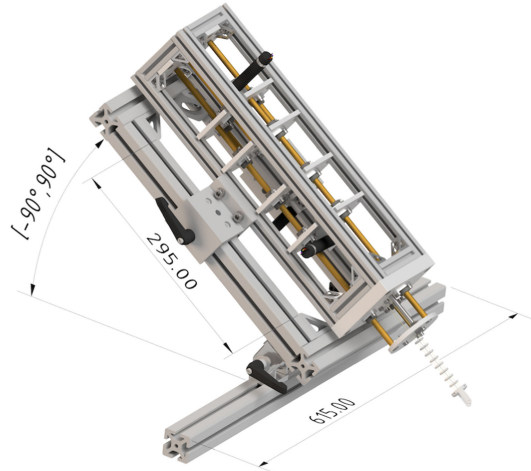


Fig. 6. Reconfigurable DoF and corresponding ranges of motion for a kinematic chain. Major dimensions in mm.

D. Reconfigurable Kinematic Chain Base Pose

In order to enable adjustment of the base poses, each chain is mounted in a mechanism that allows for a coarse manual adjustment. In the neutral setting, the three kinematic chains are mounted such that their respective tip points form an equilateral triangle that lies in a horizontal plane. Each base pose can be adjusted in three DoF (see Fig. 6):

- 1) Linear displacement in direction of the linear axis
- 2) Linear displacement perpendicular to the linear axis and in a horizontal plane
- 3) Tilt angle about the second axis of linear displacement

E. PCR Assembly

The three continuum robots are assembled to a PCR by mounting them on a prismatic triangular construct from aluminum frames as depicted in Fig. 7. The mount is designed in such a way, that the end-effector can easily be accessed from all directions.

As the neutral constellation of the three kinematic chains is designed to constitute an equilateral triangle, the end-effector reflects this property. While the current design of the presented end-effector's main purpose is to allow position and orientation measurements, it can be changed in its design to hold tools or sensors.

The kinematic design defines the connections between the end-effector and the kinematic chains to be spherical joints. However, most commercially available small-scale spherical joints have a relatively high weight and limited range of motion. To maximize the workspace, a custom 3D printed spherical joint is used (see Fig. 7). The joint is made up of a universal joint that is extended with an additional rotational DoF, yielding a spherical joint (Fig. 7). One of the brackets is simultaneously the tip of the respective continuous element in the kinematic chains. The other bracket is connected to the end-effector with a screw that it rotates about.

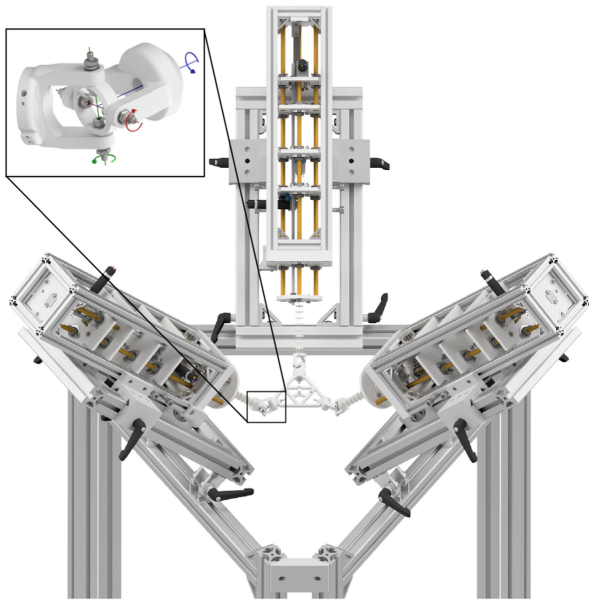


Fig. 7. Assembled spatial PCR.

IV. EXPERIMENTAL VALIDATION

Multiple experiments are conducted to assess the performance of the proposed prototype. First, a contact-free measurement method to obtain position and orientation of the end-effector is evaluated. Subsequently, the repeatability of a single continuum robot unit is examined in order to relate it to the parallel robot's repeatability, which is determined in a third experiment.

A. Experiment Design

Both the single and the parallel robot need to be measured with a contact-free measurement system due to their compliance. The chosen measurement device is a measurement arm with laser probe (FARO Edge with FARO Laser Line Probe HD, Faro Technologies Inc., Lake Mary, FL, USA). The laser probe can obtain point clouds from scanned objects and the corresponding software (FARO CAM2 Measure, FARO Technologies, Inc. Lake Mary, FL, USA) allows to detect geometric shapes in the point clouds. In order to extract the robots' spatial position and orientation, we equipped its parts with objects that can be easily scanned and 3D reconstructed.

For the single continuum robot, a cylindrical cap, that locks onto its tip, is designed. The cylinder can be identified from a point cloud. While this only uniquely identifies 5 DoF, the rotation about its axis of rotation can be neglected as such rotations usually don't occur in a single segment TACR with straight routed tendons. The PCR's end-effector is equipped with three metal spheres that can also be identified from point clouds (see Fig. 8).

Additionally, all three single robot units are equipped with a scannable 3D printed bracket (visible in Fig. 1). This bracket is mounted on a corner of each robot's frame and contains three metal spheres just like the parallel end-effector. As the transformation between the part and the robot's base is known from CAD design, the initial position and orientation of each

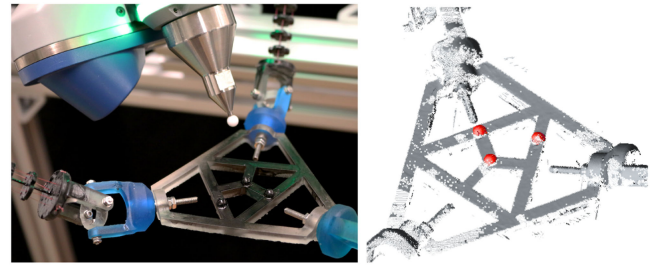


Fig. 8. Measurement of robot pose. Left: Scanning the end-effector with the a laser probe. Right: Point cloud of the scanned end-effector with extracted spheres in red.

robot in space can be determined. This allows conclusions about the shape of each continuum robot as the position and orientation of its base and the position of its tip can be computed from the scanned parts and the actuation parameters. The base frames' orientations are adjusted in a way that the tilt angle is 45° and the end-effector platform is oriented parallel to the ground.

Both experiments are preceded by a set of measurements determined to validate the measurement method. The respective robot is left in a certain pose and scanned consecutively for 20 times. From the scans, the measurement method's repeatability can be inferred which allows for an assessment of the measurement method's influence on the results. The equations to determine the repeatability are based on the ISO standard 9283:1998 [22].

In the main set of experiments, the robot moves between a pre-defined *zero configuration* and a fixed number of measured configurations. The zero configuration is defined as a configuration with a straight backbone and no linear extension for the single robot. In the parallel robot, it is set as the natural configuration the continuum robots take when the motors driving the tendons are switched off. For the single continuum robot, five configurations are considered while for the parallel robot the number is increased to ten distributed throughout the robot's workspace. For each configuration, 15 trials are performed. In between each trial, the robot is moved back into its zero configuration.

B. Results

After each experiment, the positioning and orientation repeatability can be computed for the measurement method, the zero configuration and each of the measured configurations. An overview of the experiments' results is displayed in Fig. 9. The bars show the positioning repeatability in dark grey (left y-axis) and the orientation repeatability in light grey (right y-axis). The measurement method's repeatability (first element to the left) is lower in magnitude than the measured repeatabilities ($0.65 \text{ mm}/0.72^\circ$ for single robot and $0.31 \text{ mm}/0.73^\circ$ for PCR). Moreover, most measured configurations for the parallel robot show reduced average repeatabilities $3.3 \text{ mm}/1.2^\circ$ in comparison to those measured with the single continuum robot $5.5 \text{ mm}/3.2^\circ$.

Two major phenomena can be observed from the measurements that have an effect on the repeatability: Parts of the measurements for the zero configuration are visibly clustered in

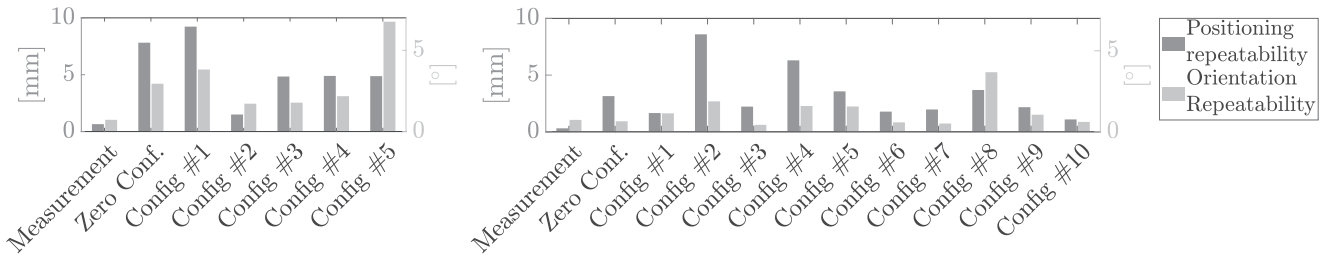


Fig. 9. Positioning and Orientation repeatability measurement results. Left: Experiments with a single continuum robot. Right: Experiments with the parallel continuum robot.

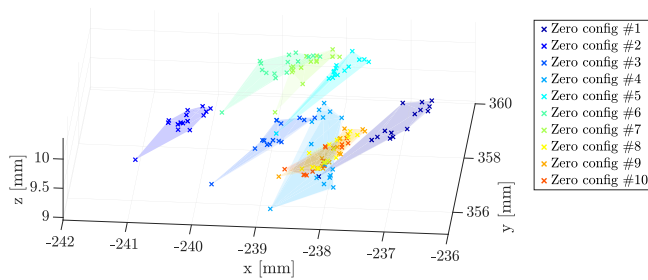


Fig. 10. Hysteresis illustrated through clustering of zero configuration measurements by the preceding command configuration. Crosses signify the end-effector center position in space, opaque areas highlight the clusters.

different spatial regions. When highlighting the measurements depending on the preceding measured configuration, different regions can be determined in the measured zero configurations (see Fig. 10). This effect is visible in both the single and the parallel robot. This is a typical occurrence of *hysteresis*, a phenomenon common to continuum robots. Because of the elastic elements, the storing and releasing of the elastic energy differs depending on the path taken to a target pose, thus influencing the actual obtained pose. Moreover, inaccuracies in the design and backlash in the motor and its gearbox can contribute to this effect.

The *multi-dimensional pose accuracy variation*, a value introduced in ISO standard 9283:1998 [22], quantifies the maximum distance between poses approached from different directions. Therefore, this is an adequate measure for hysteresis. The multi-dimensional pose accuracy variation is 6.55 mm/6.46° for a single robot and 3.61 mm/2.74° for the PCR.

The second phenomenon can be observed over the course of 15 trials per configuration. Especially for the parallel robot, a gradual shift in the obtained poses can be observed for most of the configurations. The general direction of this shift is almost constant from the first to the last cycle. Such an effect is called *drift*. Contrary to the hysteresis, the reasons for this can't be easily determined. Possible sources are:

- A loss in tendon pretension that has been observed during the experiments
- Material deterioration of 3D printed parts
- Loosening of the knots in the tendons due to high forces

TABLE I
DISTANCE BETWEEN FIRST AND LAST TRIAL FOR EACH CONFIGURATION DUE TO DRIFT

Configuration	Distance between the first and last cycle
Configuration #1	1.82 mm
Configuration #2	10.63 mm
Configuration #3	3.39 mm
Configuration #4	8.35 mm
Configuration #5	4.53 mm
Configuration #6	2.53 mm
Configuration #7	2.70 mm
Configuration #8	1.44 mm
Configuration #9	3.08 mm
Configuration #10	1.26 mm

The magnitude of this effect can be quantified through the distance between the first and last measurement for each configuration. These values are listed in Table I for the experiments with the parallel robot.

V. DISCUSSION

This section discusses the implications of the experimental results presented in the previous section. Furthermore, main advantages and possible applications of the proposed robot design are highlighted, followed by design limitations.

A. Experimental Results

The presented initial experiments show that the robot reliably repeats a commanded pose. This proves the basic functionality of the proposed design and validates the observation that the individual design elements perform well. The chosen measurement method proves to be reliable and precise enough in comparison to inaccuracies in the robot while enabling contact-free measurements.

When comparing the repeatability values of the single and the parallel robot, a major effect of the combination in a parallel kinematic structure becomes apparent. In serial robots, the errors introduced by the individual links of a robot add up, yielding an error of the complete robot that is inevitably larger than that of a single link. In parallel robots, the parallel structure prevents such a behaviour because the single links are still independent within the whole structure. This is reflected in the repeatability

as the values in the parallel prototype don't triple but rather stay of the same magnitude as the positioning repeatability of a single continuum robot. The span of repeatability values, that is between 1.5 mm and 9.2 mm for a single robot, lies between 1.1 mm and 8.6 mm for the parallel prototype. The same holds for the orientation repeatability. The values for a single continuum robot range between 1.7° and 6.8° which is comparable to the span of 0.4° to 3.7° measured in the parallel prototype. Multiple factors such as proximity to the workspace border, presence of singularities or extent of bending within the backbones can influence the specific repeatability of a configuration. The extent of the respective factors can be assessed in further dedicated experiments. An interesting observation for both repeatability measures is that the lower boundary of the span is even lower than for a single robot. Similarly, the mean values of all measured repeatabilities decrease from 5.5 mm/ 3.2° for a single continuum robot to 3.3 mm/ 1.2° for the parallel robot. The parallel structure likely plays a role in the lower repeatability as the forces exerted between the single continuum robots increase the end-effector's stiffness and reduce its free play.

This is also reflected in the calculated multi-dimensional pose accuracy variation values. As the hysteresis that is connected to these values is an element of the repeatability, the reduction of around 50% between the single and the parallel robot shows the stabilizing characteristic in parallel continuum robots. The improvement of the repeatability through parallelization of continuum robots can therefore be validated. This proves a major motivation for research on parallel continuum robots as the relatively low repeatability of continuum robots can potentially be balanced through parallelization.

B. Contributions of the Proposed Design

The proposed design serves as a proof of concept for spatial tendon-actuated parallel continuum robots. In our previous work, we investigated tendon-actuated parallel continuum robots and their advantages, but limited to a planar PCR [14]. The successful transition to a spatial PCR design provides the basis for transferring of results achieved with our planar PCR and for further investigations on kinematics, statics, and dynamics. In comparison to most other parallel continuum robots whose kinematic chains passively bend due to changes in the distance between their end points, tendon actuation provides the means to actively actuate the bending of every kinematic chain. This leads to more control over the legs' movements and more direct end-effector control.

Alternative designs possess actively bent kinematic chains that are pneumatically actuated [12], [13]. However, pneumatic actuation is more challenging to implement and to control. Furthermore, tendon-actuated continuum robots provide a number of modifiable properties which enables the investigation of the effect of design variations such as variable tendon routing [23], concatenation of multiple segments [15], [24], or variable stiffness mechanisms [25]. Thanks to the prototype's reconfigurable design, different types of tendon-actuated continuum robots can easily be implemented and compared.

Another novelty of the presented prototype is the redundancy introduced by the linear axes. It can be utilized to fulfil secondary objectives like the avoidance of parallel singularities [17], [3] or the optimization of particular kinematic properties such as stiffness or dexterity at the end-effector [18].

A possible application scenario enabled by the presented properties is the individual task space entry of the kinematic chains and subsequent coupling to the end-effector. This can be valuable in enclosed task space situations such as minimally invasive surgery or non-destructive inspection (NDI). The evaluation of such applications is enabled by the spatial reconfigurability of the kinematic chains. As the requirements of specific surgical or NDI applications highly differ, further kinematic analysis of the prototype will narrow down possible applications and allow for building and assessing targeted prototypes.

We would like to acknowledge that some of the stated contributions and possible advantages of the present PCR are currently of a hypothetical and theoretical nature and need to be verified with further kinematic analyses and experiments in the future.

C. Limitations

The hysteresis and drift effects observed in the experimental results are possible factors contributing to the robot's repeatability which can therefore be improved by reducing them. The elastic properties of the NiTi-Backbones within the continuum robots are a common factor in hysteresis as energy is stored and released when the robot bends [26]. This is a statistical factor that can hardly be avoided by design. The backlash in the motors and their gearboxes causes a potential tendon displacement of approximately 0.21 mm. Under the assumption of constant curvature in the tendons this can lead to a linear displacement of a single robot's tip of up to 1.92 mm. To reduce this error, the diameter of the 3D printed ball gear on the motors can be reduced, leading to a smaller tendon displacement but also reducing the motor's lever arm on the tendons and thus the maximum force that can be exercised on them. Alternatively a motor with a smaller transmission or smaller gear backlash can be used.

Another hysteresis factor is the 3D printed joint. While it enables a more dexterous mechanism in comparison to commercially available spherical joints, the prototypical design leaves design specifics to be improved such as the introduction of bearings or the optimization of the fit between the rotational parts. Nevertheless, the joints move as designed with little friction present. However, the specific design requires the consideration of the joints' kinematics in trajectory planning. This can prevent undesirable joint states such as configurations that include self-collision between the brackets or kinematically unstable configurations like a *gimbal lock* which can also contribute to hysteresis.

While hysteresis is a constant factor introducing an uncertainty around the target, drift unpredictably shifts the attained pose in space over time. This effect is most likely rooted within the tendons, especially the observed loss in pretension observed during the experiments. One possible cause for that would be a

gradual plastic deformation of the tendons due to intrinsic material properties or small fibers within the tendons tearing resulting in an increase in tendon length. Furthermore, the knots fixing the tendons could either open or further tighten during experiments. While the used buntline hitch knot is able to withstand high tension, spontaneous opening of knots occurred in preliminary experiments. This hints at the presence of insecure knots that may constitute a main cause for the decreasing pretension in the tendons.

VI. CONCLUSION

The proposed design initiates a new generation of parallel continuum robots by extending previous work on planar towards spatial PCR. Moreover, this is the first tendon-actuated spatial parallel continuum robot. With kinematic chains whose bending is actively controlled, the strengths of continuum robots can be deliberately used while being paired with the advantages of parallel kinematic structures. An additional linear DoF at the base of each kinematic chain enhances end-effector mobility by introducing redundancy to the parallel kinematic.

The experimental results emphasize this by showing that the parallel structure decreases the repeatability relative to a single constitutive continuum robot. Average repeatabilities of 5.5 mm in position and 3.2° in orientation in a single continuum robot can be reduced to 3.3 mm and 1.2° through the parallel coupling. Moreover, the reconfigurability of the individual kinematic chains allows for a vast adaptation of the prototype to serve in a variety of different experiments.

Therefore, this spatial tendon-actuated parallel continuum robot constitutes a basis for multiple future research directions: A design optimization can address the issues of hysteresis and drift. Implementing a kinematic model for the robot as well as integrating sensing will enable research on efficient control strategies as well as investigations on performance parameters like workspace size, singularity distribution, and robot accuracy. Furthermore, the implications of the existing kinematic redundancy of the proposed design can be investigated, which presents a yet unexplored area for parallel continuum robots.

REFERENCES

- [1] J. Burgner-Kahrs, D. C. Rucker, and H. Choset, "Continuum robots for medical applications: A survey," *IEEE Trans. Robot.*, vol. 31, no. 6, pp. 1261–1280, Dec. 2015.
- [2] K. Wen, D. Harton, T. Laliberté, and C. Gosselin, "Kinematically redundant (6 3)-dof hybrid parallel robot with large orientational workspace and remotely operated gripper," in *Proc. Int. Conf. Robot. Automat.*, 2019, pp. 1672–1678.
- [3] K. Wen and C. Gosselin, "Kinematically redundant hybrid robots with simple singularity conditions and analytical inverse kinematic solutions," *IEEE Robot. Automat. Lett.*, vol. 4, no. 4, pp. 3828–3835, Oct. 2019.
- [4] H. Jamshidifar, A. Khajepour, B. Fidan, and M. Rushton, "Kinematically-constrained redundant cable-driven parallel robots: Modeling, redundancy analysis, and stiffness optimization," *IEEE/ASME Trans. Mechatronics*, vol. 22, no. 2, pp. 921–930, Apr. 2017.
- [5] C. E. Bryson and D. C. Rucker, "Toward parallel continuum manipulators," in *Proc. Int. Conf. Robot. Automat.*, 2014, pp. 778–785.
- [6] A. L. Orekhov, C. B. Black, J. Till, S. Chung, and D. C. Rucker, "Analysis and validation of a teleoperated surgical parallel continuum manipulator," *IEEE Robot. Automat. Lett.*, vol. 1, no. 2, pp. 828–835, Jul. 2016.
- [7] C. Pacchierotti, E. M. Young, and K. J. Kuchenbecker, "Task-driven pca-based design optimization of wearable cutaneous devices," *IEEE Robot. Automat. Lett.*, vol. 3, no. 3, pp. 2214–2221, Jul. 2018.
- [8] E. M. Young and K. J. Kuchenbecker, "Implementation of a 6-dof parallel continuum manipulator for delivering fingertip tactile cues," *IEEE Trans. Haptics*, vol. 12, no. 3, pp. 295–306, Jul.–Sep. 2019.
- [9] O. Altuzarra, D. Caballero, Q. Zhang, and F. J. Campa, "Kinematic characteristics of parallel continuum mechanisms," in *Proc. Int. Symp. Adv. Robot Kinematics*, 2018, pp. 293–301.
- [10] B. Mauze *et al.*, "Nanometer precision with a planar parallel continuum robot," *IEEE Robot. Automat. Lett.*, vol. 5, no. 3, pp. 3806–3813, Jul. 2020.
- [11] Z. Yang, X. Zhu, and K. Xu, "Continuum delta robot: A novel translational parallel robot with continuum joints," in *Proc. Int. Conf. Adv. Intell. Mechatronics*, 2018, pp. 748–755.
- [12] J. A. Rivera and C. J. Kim, "Spatial parallel soft robotic architectures," in *Proc. IEEE/RSJ Int. Conf. Intell. Robot. Syst.*, 2014, pp. 548–553.
- [13] I. Singh, M. Singh, P. Pathak, and R. Merzouki, "Optimal work space of parallel continuum manipulator consisting of compact bionic handling arms," in *Proc. IEEE Int. Conf. Robot. Biomimetics*, 2017, pp. 258–263.
- [14] K. Nuelle, T. Sterneck, S. Lilge, D. Xiong, J. Burgner-Kahrs, and T. Ortmaier, "Modeling, calibration, and evaluation of a tendon-actuated planar parallel continuum robot," *IEEE Robot. Automat. Lett.*, vol. 5, no. 4, pp. 5811–5818, Oct. 2020.
- [15] E. Amanov, T.-D. Nguyen, and J. Burgner-Kahrs, "Tendon-driven continuum robots with extensible sections—a model-based evaluation of path-following motions," *Int. J. Robot. Res.*, 2019.
- [16] D. C. Rucker and R. J. Webster III, "Statics and dynamics of continuum robots with general tendon routing and external loading," *IEEE Trans. Robot.*, vol. 27, no. 6, pp. 1033–1044, Dec. 2011.
- [17] J. Kotlarski, B. Heimann, and T. Ortmaier, "Influence of kinematic redundancy on the singularity-free workspace of parallel kinematic machines," *Front. Mech. Eng.*, vol. 7, no. 2, pp. 120–134, 2012.
- [18] V. Aloï, C. Black, and C. Rucker, "Stiffness control of parallel continuum robots," in *Proc. ASME Dyn. Syst. Control Conf.*, 2018, doi: [10.1115/DSCC2018-9112](https://doi.org/10.1115/DSCC2018-9112).
- [19] J.-P. Merlet, *Parallel Robots*, 2nd ed., Berlin, Germany: SpringerNetherlands, 2006.
- [20] M. F. Grübler, *Gear theory: a theory of constrained motion and planar mechanisms*, Berlin, Germany: Springer, 1917.
- [21] K. Oliver-Butler, J. Till, and C. Rucker, "Continuum robot stiffness under external loads and prescribed tendon displacements," *IEEE Trans. Robot.*, vol. 35, no. 2, pp. 403–419, Apr. 2019.
- [22] ISO 9283:1998, "Manipulating industrial robots - performance criteria and related test methods," 1988. [Online]. Available: <https://www.iso.org/standard/22244.html>
- [23] J. Starke, E. Amanov, M. T. Chikhaoui, and J. Burgner-Kahrs, "On the merits of helical tendon routing in continuum robots," in *Proc. IEEE/RSJ Int. Conf. Intell. Robot. Syst.*, 2017, pp. 6470–6476.
- [24] M. T. Chikhaoui, S. Lilge, S. Kleinschmidt, and J. Burgner-Kahrs, "Comparison of modeling approaches for a tendon actuated continuum robot with three extensible segments," *IEEE Robot. Automat. Lett.*, vol. 4, no. 2, pp. 989–996, Jan. 2019.
- [25] M. Langer, E. Amanov, and J. Burgner-Kahrs, "Stiffening sheaths for continuum robots," *Soft Robot.*, vol. 5, no. 3, pp. 291–303, Apr. 2019.
- [26] C. Greiner-Petter and T. Sattel, "On the influence of pseudoelastic material behaviour in planar shape-memory tubular continuum structures," *Smart Mater. Struct.*, vol. 26, no. 12, 2017, Art. no. 125024.